ELSEVIER

Journal of Power Sources 81–82 (1999) 524–529

JOURNAL OF POWER SOURCES

www.elsevier.com/locate/jpowsour

Synthesis and electrochemical properties of lithium molybdenum oxides

Hironori Kobayashi [a,*], Mitsuharu Tabuchi [a], Masahiro Shikano [a], Yasuo Nishimura [a], Hiroyuki Kageyama [a], Tadashi Ishida [a], Hideo Nakamura [b], Yutaka Kurioka [b], Ryoji Kanno [c]

[a] *Osaka National Research Institute, AIST, MITI, 1-8-31 Midorigaoka, Ikeda, Osaka, 563-8577 Japan*
[b] *Department of Electrical Engineering, Faculty of Science and Technology, Kinki University, Kowakae, Osaka, 577-8502 Japan*
[c] *Department of Chemistry, Faculty of Science, Kobe University, Nada, Kobe, Hyogo, 657-8501 Japan*

Abstract

Layered oxides Li_2MoO_3 were synthesized at 923 K (sample A), 1023 K (sample B), and 1073 K (sample C) and characterized by X-ray diffractometry, magnetic and electrochemical measurements. All Li_2MoO_3 showed rhombohedral symmetry with an α-$NaFeO_2$-related structure and paramagnetic behavior down to 83 K. Lithium deintercalation from samples B and C proceeded to $x = 1.2$ in $Li_{2-x}MoO_3$. The Li/Li_2MoO_3 (samples B and C) cells showed cycling capacities of 150 mAh/g in the voltage range of 1.5–4.3 V after 10 cycles. Samples B and C showed better cycle reversibility than sample A. The different charge and discharge characteristics between samples A-C might be caused by structural differences which were indicated by X-ray diffraction measurements. © 1999 Elsevier Science S.A. All rights reserved.

Keywords: Lithium deintercalation; Layered oxide; Molybdenum oxide

1. Introduction

Layered oxides Li_2MO_3 (M = Mn, Ti, Ru, Ir, Sn, Mo) have cubic-close packed oxide-ion lattices with basal planes of octahedral interstices filled alternately by Li^+ only and by $1/3Li^+$, $2/3M^{4+}$ [1–10]. Of these 4d and 5d transition metal components, the $Ru^{5+/4+}$, $Ir^{5+/4+}$, and $Mo^{5+/4+}$ couples permit lithium extraction from the host structure [1,9–14]. Previously, we studied structural changes with delithiation and electrochemical behavior in the $Li_{2-x}RuO_3$ system. The Li/Li_2RuO_3 cells showed excellent reversibility in the voltage range of 3.0–4.0 V with an energy density of 160 mAh/g [13]. The layered oxides $Li_{1.8}Ru_{0.6}Fe_{0.6}O_3$ and Li_2IrO_3 were also synthesized and the $Li/Li_{1.8}Ru_{0.6}Fe_{0.6}O_3$ and Li/Li_2IrO_3 cells showed the energy density of 100 and 120 mAh/g, respectively, in the voltage range of 2.0–4.3 V [10].

Fig. 1 shows the relationship between the ionic radii of M^{4+} (M = transition metals) cations and the lattice symmetry of Li_2MO_3 [15]. Li_2MoO_3 show rhombohedral symmetry and its structure has a cationic ordering that 1/3 Li and 2/3 Mo distribute randomly in the $LiMo_2$ layers [9]. James and Goodenough [9] determined the structure of Li_2MoO_3 to be an α-$NaFeO_2$-related structure using neutron Rietveld analysis. The existence of Mo_3O_{13} clusters was suggested by the He–I photoelectron spectroscopy. Hibble and Fawcett [16] and Hibble et al. [17] clarified the presence of Mo_3O_{13} clusters in Li_2MoO_3 using EXAFS and total neutron scattering measurements. While the electrochemical and chemical deintercalation of lithium from Li_2MoO_3 has been reported [9,11,12], the relationship between the crystal structure and charge-discharge cycle performance has not been understood.

In the present study, we synthesized the Li_2MoO_3 and clarified the relationship between the synthesis condition, crystal structure, and electrochemical properties.

2. Experimental

Li_2MoO_3 was synthesized from Li_2MoO_4 under a hydrogen gas flow at 823-1223 K for 24–48 h. The starting material of Li_2MoO_4 was prepared by heating the mixture of appropriate molar ratios of Li_2CO_3 and MoO_3 (Li_2CO_3: Wako Chemicals, > 99.0% purity; MoO_3: Koujundo Chemicals, > 99.9% purity).

X-ray diffraction (XRD) patterns of the powdered samples were obtained with an X-ray diffractometer (Rigaku Rotaflex/Rad-C) with Cu$K\alpha$ radiation. XRD data for

* Corresponding author

0378-7753/99/$ - see front matter © 1999 Elsevier Science S.A. All rights reserved.
PII: S0378-7753(98)00227-4

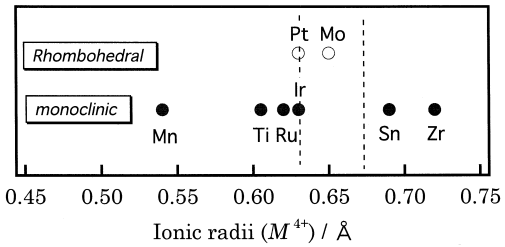

Fig. 1. Relationship between ionic radii of transition metals (M^{4+}) and lattice symmetry of Li_2MO_3. Rhombohedral and monoclinic lattice symmetry are represented by ○ and ●, respectively.

Rietveld analysis were collected for 1–2 s at each 0.02° step width over a 2θ range from 15 to 100°. The structural parameters were refined by Rietveld analysis using the computer program RIETAN97-BETA [18].

Magnetic susceptibility was measured by a Faraday balance (Shimadzu, MB-3) between 83 and 293 K. Mn Tutton's salt ($(NH_4)_2Mn(SO_4)_2 \cdot 6H_2O$) was used as the standard substance for magnetic susceptibility. Data were corrected by subtraction of closed shell diamagnetism.

Electrochemical intercalation and deintercalation were carried out using lithium cells with a coin-type configuration. The working electrode consisted of a mixture of 45–75 mg samples, 15–20 mg acetylene black, and 0.3 mg Teflon powder. The mixture was pressed into a tablet of 15 mm diameter under a pressure of 5 kgf/cm^2. The counter electrode was a 15 mm diameter and 1 mm thickness disk of lithium metal. A microporous polypropylene sheet was used as the separator. The electrolyte used in these cells was 1 M solution of $LiClO_4$ in a 50:50 mixture of ethylene carbonate (EC) and 1,2-dimethoxycarbonate (DMC) (Toyama Petrochemical, battery grade). The cells were constructed in an argon filled glove-box. The current density was calculated based on the cathode area. The electrochemical measurements were carried out at room temperature after standing overnight under zero current flow. Cell properties were measured galvanostatically using a MacPile II (Bio-Logic).

3. Results and discussion

3.1. Synthesis

Fig. 2 shows the X-ray diffraction (XRD) patterns for Li_2MoO_3 synthesized at various conditions under a hydrogen gas flow. Sample synthesized at 823 K showed a small amount of unreacted Li_2MoO_4, while the samples synthesized above 1123 K contained Mo metal. Monophasic property of Li_2MoO_3 was synthesized at 923 K (sample A), 973 K (sample B), and 1073 K (sample C). All the XRD peaks could be indexed by a hexagonal lattice similar to that of α-$NaFeO_2$. The splitting of the peaks indexed as 006 and 101 reflections as shown in Fig. 2, which are characteristics for layered structure, became clearer with increasing synthesis temperature. The Li/Mo ratio of samples A–C was determined to be 2.00:1.00 by ICP emission spectrometry. The composition was thus confirmed to be Li_2MoO_3 where Mo ions are in 4+ valence states.

3.2. Structure

The structure of Li_2MoO_3 synthesized at 923–1073 K was refined with space group $R\bar{3}m$ using a structural model reported by James and Goodenough [9], Mo at 3*b*

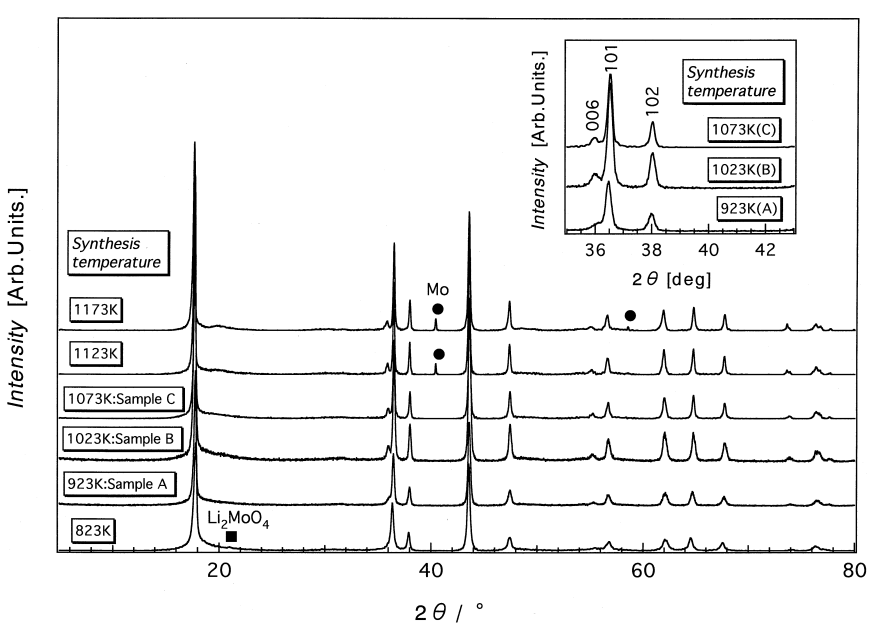

Fig. 2. X-ray diffraction patterns for Li_2MoO_3 synthesized under a hydrogen gas flow at various conditions. Impurity phases of Mo and Li_2MoO_4 are indicated by ● and ■, respectively. XRD patterns in the range of $35° < 2\Theta < 43°$ are also shown inside figure.

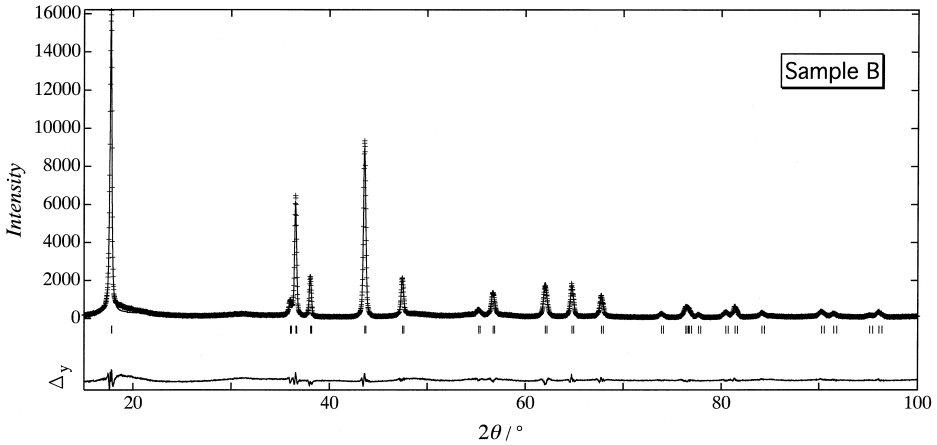

Fig. 3. Rietveld refinement results for Li_2MoO_3 (sample B). Observed, calculated, and difference patterns are shown.

(0,0,0.5), Li(1) at 3*b* (0,0,0.5), Li(2) at 3*a* (0,0,0), O at 6*c* (0,0, *z*) with $z \sim 0.25$. At first, we assumed that a small amount of molybdenum ions existed in the 3*a* site, but site occupation parameter of *g* was led to a negative value for all samples. Therefore, the site occupation parameters of Mo, Li(1), and Li(2) were fixed at 0.667, 0.333, and 1.0, respectively. The overall thermal parameters *B* for all sites were constrained to be the same value. No correction was made for preferred orientation. Fig. 3 shows the typical Rietveld analysis results of sample B. Table 1 lists final *R* factors, lattice and structural parameters, and their estimated standard deviations. From the viewpoint of α-$NaFeO_2$ structure, Li_2MoO_3 could be expressed to be $(Li)_{3a}(Mo_{0.667}Li_{0.333})_{3b}O_2$. Fig. 4 shows the synthesis temperature dependence of lattice parameters. The *a* axis parameter decreased and *c* axis parameter increased with synthesis temperature. These lattice parameters obtained after Rietveld analysis are close to $a = 2.881(2)$ and $c = 14.93(1)$ Å reported by Gopalakrishnan and Bhat [11], but are a little different from $a = 2.891(1)$ and $c = 14.81(1)$ Å reported by James and Goodenough [9] and $a = 2.884(1)$ and $c = 14.834(2)$ Å reported by Kumada et al. [12]. All the XRD patterns reported as references are similar to that of sample A with no splitting of 006 and 101 reflections

Table 1

(a) Structural parameters for Li_2MoO_3 (sample A)

$a = 2.87778(11)$ Å, $c = 14.9458(9)$ Å, $B = 2.03(6)$ Å^2, $R_{wp} = 18.45\%$, $R_e = 5.51\%$, $R_I = 6.89\%$, $R_F = 3.95\%$

Atom	Site	*g*	*x*	*y*	*z*
Mo	3*b*	0.667	0	0	0.5
Li(1)	3*b*	0.333	0	0	0.5
Li(2)	3*a*	1	0	0	0
O	6*c*	1	0	0	0.2451(3)

(b)Structural parameters for Li_2MoO_3 (sample B)

$a = 2.87564(10)$ Å, $c = 14.9586(8)$ Å, $B = 1.89(6)$ Å^2, $R_{wp} = 18.08\%$, $R_e = 5.56\%$, $R_I = 7.00\%$, $R_F = 3.97\%$

Atom	site	*g*	*x*	*y*	*z*
Mo	3*b*	0.667	0	0	0.5
Li(1)	3*b*	0.333	0	0	0.5
Li(2)	3*a*	1	0	0	0
O	6*c*	1	0	0	0.2452(3)

(c) Structural parameters for Li_2MoO_3 (sample C)

$a = 2.87451(9)$ Å, $c = 14.9671(7)$ Å, $B = 1.82(6)$ Å^2, $R_{wp} = 18.65\%$, $R_e = 5.55\%$, $R_I = 7.33\%$, $R_F = 4.15\%$

Atom	site	*g*	*x*	*y*	*z*
Mo	3*b*	0.667	0	0	0.5
Li(1)	3*b*	0.333	0	0	0.5
Li(2)	3*a*	1	0	0	0
O	6*c*	1	0	0	0.2452(3)

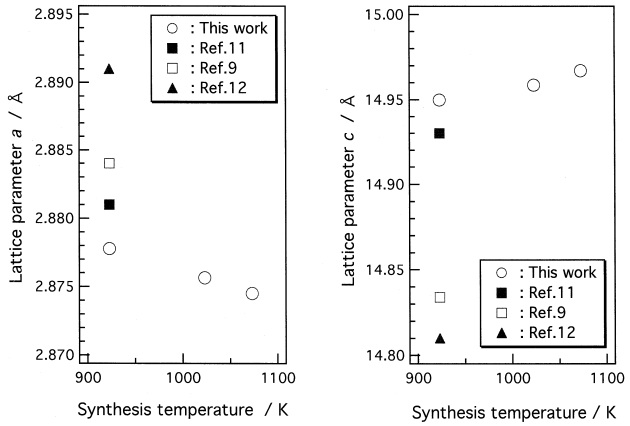

Fig. 4. Synthesis temperature dependence of the lattice parameters a and c for Li_2MoO_3. Data have been reported as references are also plotted.

[11,12]. The clear splitting of 006 and 101 reflections seem to correspond the ideal layered structure. In this study, we synthesized Li_2MoO_3, which are closer to the ideal layered structure than other samples reported. From the structural analysis, we detected the decreases of Mo–Mo bond distances from 2.8778(1) to 2.8745(1) Å and no change of Mo–O distances of 2.034(3) Å with synthesis temperature.

3.3. Physical properties

The electrical resistivity was measured by d.c. two-probe method at room temperature. Li_2MoO_3 (sample B) showed the high resistivity of $\rho > 100$ kΩ m. The magnetic field dependence of the magnetization at 83 and 293 K suggested no existence of a spontaneous magnetization from ferromagnetic impurity for all samples. Fig. 5 shows the temperature dependence of inverse magnetic susceptibility, χ_m^{-1}, at 12.5 kOe in the range of 83–293 K. All samples showed the Curie–Weiss like paramagnetic behavior above 163 K. Therefore, the effective magnetic moments of μ_{eff} were calculated using an equation $\chi_m^{-1} = (T - \theta)/C_m$ (C_m: Curie constant, θ: Weiss temperature) from the data above 163 K. Magnetic parameters, μ_{eff} and θ, are summarized in Table 2. For all the samples, the μ_{eff} was observed around 0.62 μ_B. The value of 0.62 μ_B was far from that of 2.83 μ_B expected with two unpaired 4d electrons of Mo^{4+} assuming the spin-only contribution for the magnetic moment.

3.4. Electrochemical properties

Figs. 6 and 7 show the charge and discharge curves in the voltage range of 1.5–4.3 V. When a current density of 0.2 mA/cm^2 was used as shown in Fig. 6(b), the extraction of lithium from sample B proceeded from $x = 0$ (Li_2MoO_3) to $x = 1.2$ ($Li_{0.8}MoO_3$), which corresponded to a valence change from Mo^{4+} to $Mo^{5+/6+}$. Sample B showed the discharge capacity of 200 mAh/g for the 1st cycle and 150 mAh/g for the 10th cycles, while sample A showed the discharge capacity of 190 mAh/g for the 1st cycle and 110 mAh/g for the 10th cycles. For both samples, significant capacity loss was observed after the 1st cycle and the average discharge voltage was around 2.4 V. In comparison with sample A, sample B synthesized at higher temperature showed better cycle reversibility. When a current density of 0.5 mA/cm^2 was used as shown in Fig. 7, charge and discharge curves of samples B and C showed the similar behavior. The discharge capacity of both samples was about 150 mAh/g for the 1st cycle and was about 100 mAh/g for the 10th cycles. For sample B, the discharge capacity for 10 cycles decreased from 170 to 100 mAh/g with increasing current density from 0.2 to 0.5 mA/cm^2. XRD data for the samples after 10 cycles showed that Li_2MoO_3 kept the layered structure with broader peaks.

3.5. Discussion

Previously we reported physical properties of the layered oxide Li_2RuO_3 [13,14]. Li_2RuO_3 has monoclinic symmetry with Ru^{4+} hexagonal networks in successive $LiRu_2$ layers. The effective magnetic moment of Li_2RuO_3 suggested that one half of 4d spin were delocalized in Li_2RuO_3 and this result corresponded to the relative low resistivity of 0.1 Ωm. In Li_2MoO_3, the effective magnetic moments suggested that most parts of the 4d electrons of Mo^{4+} were delocalized, while Li_2MoO_3 showed high resistivity. These physical properties may reflect the characteristics of Mo_3O_{13} clusters with a disordered arrangements in Li_2MoO_3 reported by Hibble and Fawcett [16] and Hibble et al. [17] because paramagnetism and high resistivity are similar to diamagnetism and semiconducting, which could be explained on Mo_3O_{13} clusters models by James and Goodenough [9]. There is one possible explanation that conductivity path is separated by clusters though the 4d electrons are delocalized inside clusters. A

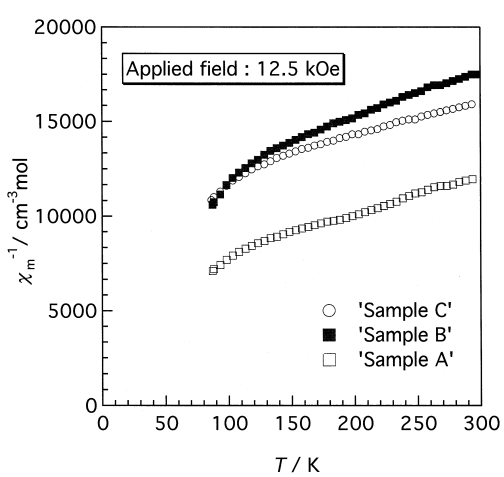

Fig. 5. Temperature dependence of inverse magnetic susceptibility for Li_2MoO_3 measured at the temperature from 83 to 300 K in the magnetic field of 12.5 kOe.

Table 2
Magnetic parameters for Li_2MoO_3

Samples	Effective magnetic moment, μ_{eff}/μ_B	Weiss temperature, θ/K	Regions obeyed the Curie–Weiss law/K
A	0.62	−289	163–288
B	0.57	−426	163–288
C	0.67	−614	163–288

slightly large overall thermal parameters may indicate that the atomic positions are a little deviation from those determined from Rietveld analysis, caused by the formation of disordered clusters.

From the viewpoint of electrochemical properties, the different 1st charge curves in the voltage range of 3.0–3.8 V, observed between samples A–C, may reflect that the real structure is more complex than that represented by an α-$NaFeO_2$-related structure. These charge curves, corresponding to the different lattice parameters and magnetic susceptibility, seem to reflect the different diffusion velocity affected by an arrangement of Mo_3O_{13} clusters. In addition, the capacity loss after the 1st cycle may be caused by a decomposition of the layered structure of Li_2MoO_3 in the 1st charge run. A small amount of Mo ion migrated to Li cite during first several charge–discharge process and stable structure obtained after several cycles permit reversible charge–discharge process. This explanation seem to be consistent with the result that a small amount of Mo ion migrated to 3*a* cite for Li ion in $Li_{0.9}MoO_3$ using neutron Rietveld analysis [9]. Perhaps it is *correct* to say that the increase of synthesis temperature makes the MoO_6 layers to be stable against the migration of $Mo^{5+/6+}$ in charge–discharge cycle run and, therefore, different cycle performances were observed between samples A and B. There are a variety of lithium molybdenum oxides with structures suitable for the diffusion of Li ions. By investigating these compounds and synthesizing new

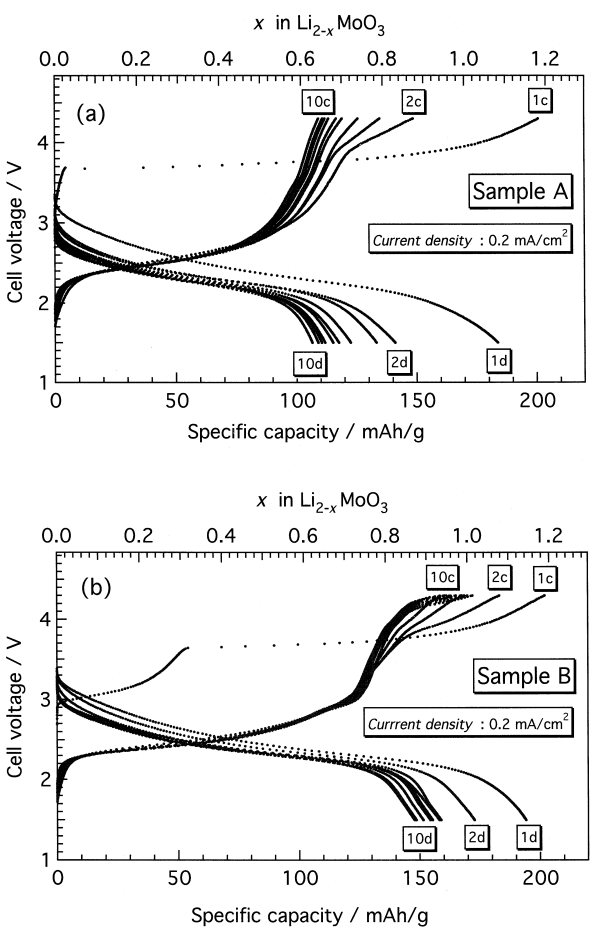

Fig. 6. Charge and discharge curves of the cells, Li/sample A (a) and Li/sample B (b), as a function of x in $Li_{2-x}MoO_3$ (top axis) and the energy density (bottom axis) with a current density of 0.2 mA/cm^2. Cut-off voltages are between 1.5 and 4.3 V.

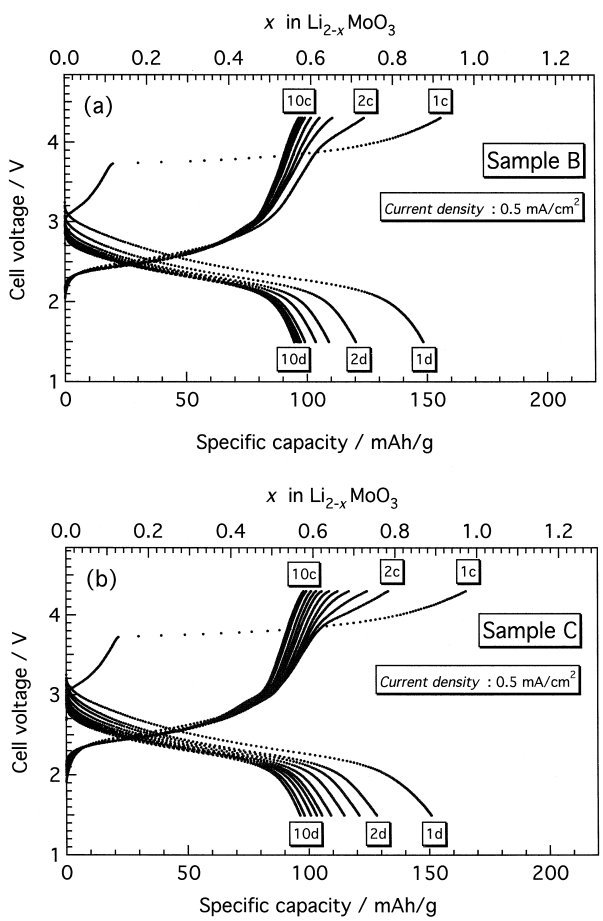

Fig. 7. Charge and discharge curves of the cells, Li/sample B (a) and Li/sample C (b), as a function of x in $Li_{2-x}MoO_3$ (top axis) and the energy density (bottom axis) with a current density of 0.5 mA/cm^2. Cut-off voltages are between 1.5 and 4.3 V.

solid solutions systematically, there is possibility to promising cathode materials for lithium secondary batteries.

4. Conclusions

In the present study, the layered oxides Li_2MoO_3 were synthesized at various conditions and Li_2MoO_3, which is close to the ideal α-$NaFeO_2$-related structure, were obtained at 1023–1073 K. The Li/Li_2MoO_3 cells showed cycle reversibility with the cycling capacities of 150 mAh/g in the voltage range of 1.5–4.3 V after 10 cycles. A little different lattice parameter with synthesis temperature seem to reflect different charge–discharge characteristics between samples A–C.

References

[1] A.C.W.P. James, J.B. Goodenough, J. Solid State Chem. 74 (1988) 287–294.
[2] P. Strobel, B. Lambert-Andron, J. Solid State Chem. 75 (1988) 90–98.
[3] J.F. Dulac, C.R. Acad. Sci., Paris, Ser. B 270 (1970) 223–226.
[4] M. Jansen, R. Hoppe, Z. Anorg. Allg. Chem. 397 (1973) 279–289.
[5] A. Riou, A. Lecerf, Y. Gerault, Y. Cudennec, Mater. Res. Bull. 27 (1992) 269–275.
[6] J.F. Dorrian, R.E. Newnham, Mater. Res. Bull. 4 (1969) 179–184.
[7] V.G. Lang, Z. Anorg. Allg. Chem. 348 (1966) 246–256.
[8] J.L. Hodeau, M. Marezio, A. Santoro, R.S. Roth, J. Solid State Chem. 45 (1982) 170–179.
[9] A.C.W.P. James, J.B. Goodenough, J. Solid State Chem. 76 (1988) 87–96.
[10] H. Kobayashi, R. Kanno, M. Tabuchi, H. Kageyama, O. Nakamura, M. Takano, J. Power Sources 68 (1997) 686–691.
[11] J. Gopalakrishnan, V. Bhat, Mater. Res. Bull. 22 (1987) 769–774.
[12] N. Kumada, S. Muramatsu, N. Kinomura, F. Muto, J. Ceram. Soc. Jpn. 96 (1988) 1181–1185.
[13] H. Kobayashi, R. Kanno, Y. Kawamoto, M. Tabuchi, O. Nakamura, M. Takano, Solid State Ionics 82 (1995) 25–31.
[14] H. Kobayashi, R. Kanno, Y. Kawamoto, M. Tabuchi, O. Nakamura, Solid State Ionics 86–88 (1996) 859–863.
[15] R.D. Shannon, C.T. Prewitt, Acta Crystallogr. B 25 (1969) 925–946.
[16] S.J. Hibble, I.D. Fawcett, Inorg. Chem. 34 (1995) 500–508.
[17] S.J. Hibble, I.D. Fawcett, A.C. Hannon, Acta Crystallogr. B 53 (1997) 604–612.
[18] F. Izumi, The Rietveld Method, in: R.A. Young (Ed.), Chap. 13, Oxford Univ. Press, Oxford, 1993.